

Article

A Double Layer Sensing Electrode “BaTi_(1-x)Rh_xO₃/Al-Doped TiO₂” for NO₂ Detection above 600 °C

Bilge Saruhan *, Azhar A. Haidry †, Ayhan Yüce, Engin Ciftiyürek and Guillermo C. Mondragón Rodríguez †

German Aerospace Center, Institute of Materials Research, Linder Hoehe, 51147 Cologne, Germany; aa.haidry@nuaa.edu.cn (A.A.H.); ayhan_yuce@hotmail.com (A.Y.); enginciftiyurek@gmail.com (E.C.); guillermo.mondragon@cidesi.edu.mx (G.C.M.R.)

* Correspondence: bilge.saruhan@dlr.de; Tel.: +49-2203-601-3228; Fax: +49-2203-696-480

† These authors contributed equally to this work.

Academic Editor: Russell Binions

Received: 8 December 2015; Accepted: 15 April 2016; Published: 29 April 2016

Abstract: NO₂ emission is mostly related to combustion processes, where gas temperatures exceed far beyond 500 °C. The detection of NO₂ in combustion and exhaust gases at elevated temperatures requires sensors with high NO₂ selectivity. The thermodynamic equilibrium for NO₂/NO ≥ 500 °C lies on the NO side. High temperature stability of TiO₂ makes it a promising material for elevated temperature towards CO, H₂, and NO₂. The doping of TiO₂ with Al³⁺ (Al:TiO₂) increases the sensitivity and selectivity of sensors to NO₂ and results in a relatively low cross-sensitivity towards CO. The results indicate that NO₂ exposure results in a resistance decrease of the sensors with the single Al:TiO₂ layers at 600 °C, with a resistance increase at 800 °C. This alteration in the sensor response in the temperature range of 600 °C and 800 °C may be due to the mentioned thermodynamic equilibrium changes between NO and NO₂. This work investigates the NO₂-sensing behavior of duplex layers consisting of Al:TiO₂ and BaTi_(1-x)Rh_xO₃ catalysts in the temperature range of 600 °C and 900 °C. Al:TiO₂ layers were deposited by reactive magnetron sputtering on interdigitated sensor platforms, while a catalytic layer, which was synthesized by wet chemistry in the form of BaTi_(1-x)Rh_xO₃ powders, were screen-printed as thick layers on the Al:TiO₂-layers. The use of Rh-incorporated BaTiO₃ perovskite (BaTi_(1-x)Rh_xO₃) as a catalytic filter stabilizes the sensor response of Al-doped TiO₂ layers yielding more reliable sensor signal throughout the temperature range.

Keywords: TiO₂; Al-doping; NO₂ sensor; BaTi_(1-x)Rh_xO₃ catalytic filter; sputtering; screen printing

1. Introduction

As compared with other emission pollutants, the amount of NO_x generated by combustion processes is very high in the atmosphere and the increase of NO_x and derivatives damage the upper atmospheric ozone layer which provides a protective shield acting as a filter to UV radiation coming from the sun. Moreover, NO_x may react with atmospheric water resulting in the formation of acid rain [1].

In case of complete combustion, the reactant burns in oxygen, producing a limited number of products. When a hydrocarbon burns in pure oxygen, the stoichiometric reaction will only yield carbon dioxide and water as well as nitrogen oxides (NO_x). Incomplete fuel oxidation yields nitrogen oxides (NO_x), mainly unburned hydrocarbons (HC), carbon monoxide (CO), CO₂, and water [2,3]:



Nitrogen oxides need to be converted over noble metal-containing catalysts to harmless compounds such as N_2 , H_2O , and CO_2 . Despite the presence of a catalyst, for instance a three-way-catalytic converter in automotive exhausts, the conversion is not always completed to fully eliminate NO and/or NO_2 . The resulting emission still contains toxic greenhouse gases.

NO_x concentrations in diesel exhausts vary typically between 50 ppm up to 1000 ppm [4]. If concentrations are given in mass units, NO_x is usually expressed as NO_2 equivalent [4]. Catalytic converters reduce exhaust gas emission below a level foreseen by regulations in order to protect human life [5,6].

Although modern vehicles are getting cleaner due to improved engines and better emission controls, this holds only when engine and converter are in proper condition. When an engine is not at maximum efficiency, consequently performance is lost, fuel is wasted, and air pollutant emissions increase. Typically, in order to adjust the fuel-efficiency, excess air (or oxygen) is added in diesel engines during combustion. Additionally, emissions will increase drastically when defects occur in a catalytic converter for instance by engine misfire or due to the driving-related issues. These may remain unnoticed if the vehicles have no integrated emission control system. Onboard diagnostic (OBD), which is in vehicles since 1996, can detect emission problems of a car or truck. OBD systems are designed to alert the driver when a component in the engine management or exhaust system begins to deteriorate or malfunction. Early detection of minor problems can often prevent more costly damage to components, such as the catalytic converter or even the engine itself. Systems such as OBD rely on multiple gas sensors controlling the exhaust condition and emissions [7].

Generally, metal oxide semiconducting (MO_x) materials are employed for the detection of various oxidizing and reducing gases due their wide applicability and with simple and cheap fabrication [8]. Despite having many benefits, limited working temperature range and poor selectivity are two main drawbacks highlighted in the literature [9–11]. At lower temperatures (below 150 °C) and at temperatures above 400 °C, the sensing properties of the semiconducting materials are reduced drastically due to decreased conductivity and/or thermal instabilities [10–13].

A large amount of efforts are being spent by current research and development to address such issues in order to broaden the application spectrum of semiconducting oxides in high-tech industries. The most widely utilized semiconducting oxides are SnO_2 , WO_3 , ZnO , and TiO_2 [10–19]. Among those, TiO_2 -based thin films and layers are reported to be more stable at higher temperatures and the stability can be further improved by bulk doping and by surface decorating with suitable cations [10,13,15–20]. In a previous study [10], we demonstrated that Al-doped TiO_2 sensor layers can detect NO_2 up to 800 °C in the concentration range of 50 ppm to 200 ppm, but the sensor response alters from the n-type at 600 °C to the p-type at 800 °C. Studying the reasons causing this change in sensor response, we demonstrated that this correlates well with the NO_2/NO thermodynamic equilibrium change occurring at temperatures above 600 °C.

Typically, the MO_x -containing resistive sensors yield signals in opposite directions toward NO and NO_2 . Thus, such changes in the high-temperature environmental condition are detrimental for diagnostic sensors and impair their long-term reliability. A common trend of improving the chemical stability and selectivity of this type of sensors is the use of a catalytic layer that acts as a catalyst, a sequestration barrier or a physical or chemical filter for undesired gases [21,22]. Hence, in order to maintain a reasonable sensitivity, better chemical stability and reliable sensor response with MO_x sensor layers at elevated temperatures, the use of an additional catalytic filter or layer may be necessary and useful. Previously, it was reported that mesoporous and noble metal-containing catalytic filters can improve the sensing ability of semiconductors [21,22]. The use of SnO_2/CeO_2 duplex layers is shown to yield improved CO-response when the sensor is exposed to heavily-reducing gas mixtures (*i.e.*, methane and/or other hydrocarbons) [23]. Hübner *et al.* [24] demonstrated later that a $BaTi_{1-x}Rh_xO_3$ catalytic layer on the surface of SnO_2 sensor layer can eliminate the sensitivity towards hydrogen when exposed to high humidity CO + H_2 gas mixture while maintaining the selectivity towards CO. Our recent report indicates that La-based complex perovskite ($LaFeCoPdO_3$) layers deposited on sputtered TiO_2 sensor layers enable the hold of their sensing ability despite aging in a harsh exhaust environment at 850 °C [25].

The current context follows this type of an approach where a $\text{BaTi}_{0.95}\text{Rh}_{0.05}\text{O}_3$ perovskite layer is combined with the Al-doped TiO_2 (Al:TiO₂) sensing layer in order to achieve a sensor array that can be integrated in catalytic converter monoliths of vehicles and, thus, allowing reliable monitoring of NO_2 emission in exhaust environments at temperatures exceeding 600 °C. Such sensor arrays will be placed within the catalytic converter of a vehicle and, therefore, must detect NO_2 with long-term selectively over a threshold concentration by withstanding these harsh conditions (*i.e.*, thermal aging caused by high gas flow rates and elevated temperatures). An adaptive and self-regenerative catalyst such as this can provide a thermal protection for the MO_x-based sensing layer, as well as enabling a reliable sensor response toward NO_2 at temperatures as high as 900 °C.

2. Experimental Section

2.1. Synthesis of Al-Doped TiO_2 Layers by Sputtering

Al-doped TiO_2 thin layers were deposited via a reactive magnetron radio frequency (RF) sputtering technique from metallic targets using oxygen as a reactive gas and without applying any heating of the substrate or system. Sputtering equipment (from von Ardenne GmbH, Dresden, Germany) with two sputter sources was used to deposit the coatings in an argon + oxygen gas mixture. Al-doped TiO_2 thin layers were deposited on the polished Al_2O_3 sensor platforms, onto which the interdigitated Pt-circuits were previously deposited by screen-printing. For the deposition of Al-doped TiO_2 , two metallic targets, *i.e.*, Ti (99.95% pure) and Al (99.99% pure) were used and were placed face to face in a plasma reactor chamber. During the coating process, the substrate holder was rotated at 13 rpm. This rotational movement enables the homogenous distribution of aluminum in the TiO_2 matrix. A power of 80 W at the Al target and 500 W at the Ti target yielded 4.64 at.% Al in TiO_2 . The partial pressure of argon and oxygen during the coating was 27.4 and 5.7 sccm, respectively. After 12 h of sputtering process, an Al-doped TiO_2 coating with a thickness of 1.2 μm was achieved. Pt-interdigitated electrodes (IDEs) are composed of two connection tracks having 300 μm -wide interlaces with bands/gaps of 300 μm from each other on alumina substrates (see Figure 1). The employed (IDE) sensor design requires no heater at the backside of the sensor platforms. Simultaneously, we deposited thin undoped and Al-doped TiO_2 layers (*ca.* 1–1.5 μm) onto the sapphire single crystal substrates in order to enable XRD measurements without any interference from the polycrystalline alumina substrate material.

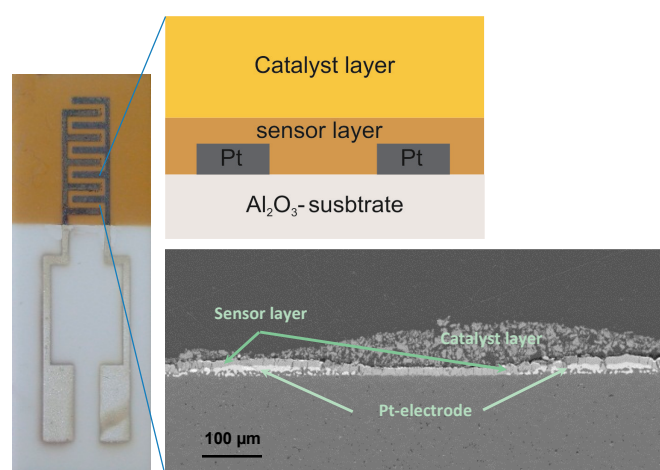


Figure 1. Sensor platform consisting of interdigitated Pt-electrodes (IDE), a semiconducting oxide sensor layer, and a catalytic filter layer. The SEM micrograph shows these layers in the cross-section as above, schematically specified: top layer: $\text{BaTi}_{0.9}\text{Rh}_{0.1}\text{O}_3$ catalytic layer, middle layer: Al-doped TiO_2 sensor layer and bottom layer: Pt-electrode on alumina substrate.

2.2. Synthesis of the Catalysts

Ba-acetate ($\text{Ba}(\text{C}_2\text{H}_3\text{O}_2)_2$, 98% Chempur), Ti-isopropoxide ($\text{Ti}\{\text{OCH}(\text{CH}_3)_2\}_4$, 99.999% Aldrich), and Rh-nitrate ($\text{Rh}(\text{H}_2\text{O})(\text{OH})_{3-y}(\text{NO}_3)_y$, $y=2-3$) were employed as starting chemicals to prepare the $\text{BaTi}_{(1-x)}\text{Rh}_x\text{O}_3$ perovskite. Barium acetate was dissolved in acetic acid and Ti-isopropoxide was diluted with isopropanol and acetyl-acetone solution. Barium and Ti sols were homogeneously mixed and then the Rh-nitrate solution was added to this mixture. The amount of the aqueous Rh-nitrate was calculated to obtain perovskite powders of the following composition $\text{BaTi}_{0.9}\text{Rh}_{0.1}\text{O}_3$. The solvents were slowly evaporated under constant stirring at room temperature. The catalysts were finally calcined in a furnace under static air up to $1000\text{ }^\circ\text{C}$ for 5 h with a heating rate of $10\text{ }^\circ\text{C min}^{-1}$ [26].

The catalytic powder was then milled and mixed with some binder for screen printing on the interdigitated electrode sensor platforms and/or on the Al-doped TiO_2 sensing layer, which was previously sputtered on Pt-interdigitated electrodes.

2.3. Sensor Array Layout

Sensor platforms were fabricated by deposition of sensing layer on interdigitated Pt-electrodes (IDE) which were deposited previously on Al_2O_3 substrates as shown in Figure 1, left. The catalytic filter was then brought on the sensor layer by means of screen printing as thick and porous layer (see Figure 1, bottom).

2.4. Characterization Methods

Al-doped TiO_2 sensing layers and $\text{BaTi}_{0.9}\text{Rh}_{0.1}\text{O}_3$ catalytic powder layers are investigated by SEM/EDX for their compositions and by X-ray powder diffraction method (XRD) for the phase condition.

Microstructure and morphology analysis of the sensing electrodes in terms of porosity, grain size, and surface condition were done by means of FE-SEM (Carl Zeiss Microscopy, Ultra 55, Oberkochen, Germany). EDX analysis were carried out by GEMINI (Oxford Inst. GmbH, Wiesbaden, Germany). The XRD diffractograms of the catalysts were obtained in a diffractometer D5000 from SIEMENS with $\text{Cu K}\alpha$ radiation ($\lambda = 1.54178\text{ \AA}$). The reflections from the JCPDS (Joint Committee on Powder Diffraction Standards) database were assigned to the experimental diffractograms with the program EVA from BRUKER AXS. Scanning Electron Microscopic (SEM) analysis of the catalysts was carried out in a Zeiss Ultra 55 microscope equipped with an Energy Dispersive X-ray Spectrometer (EDS) from Oxford Instruments. For high-temperature XRD measurement of $\text{BaTi}_{0.95}\text{Rh}_{0.05}\text{O}_3$ catalyst, the specimens were prepared by packing powder in $\text{Ø} 25\text{ mm}$ alumina crucible. Data collection time was 30 s per scan. The test powders were initially calcined at $700\text{ }^\circ\text{C}$ prior to *in situ* high-temperature X-ray diffraction (HT-XRD) measurements.

Sensing characterization was carried out in a specially constructed apparatus consisting of a tube furnace with cascade control and a custom-built quartz glass reactor providing a thermocouple directed at the specimen. The composition of the mixed gas was controlled by an eight-channel mass flow controller (MFC-647b from MKS Instruments GmbH). The gas flow rate was adjusted to 400 mL/min and the NO_2 concentrations were varied between 50 and 200 ppm. Mostly argon was used as the carrier gas. In some of our experiments, synthetic air ($80\% \text{ N}_2 + 20\% \text{ O}_2$) was employed as the carrier gas indicated relevantly. The DC electrical measurements were carried out by using a Keithley 2635A Sourcemeter, with a computer-controlled LabView program. A constant current of $1 \times 10^{-6}\text{ A}$ was applied during all sensor measurements. Steady-state gas response measurements were started under a constant carrier gas flow. These sensors were initially exposed to a constant flow of carrier gas to equilibrate the operating conditions. After a stable baseline was reached, the target gas was introduced into the chamber, continuously flowing with a constant for 40 min at the end of which the NO_2 -gas flow was ceased and only carrier gas is let flown through. These two steps were repeated for 50, 100, and 200 ppm NO_2 and/or CO gas concentrations.

3. Results and Discussion

3.1. Al-Doped TiO₂ Sensor Layer

As the XRD investigation of the as-coated and *ex situ* at 500 °C, 800 °C, and 1000 °C heat-treated Al-doped TiO₂ layers indicate, the layer is weakly crystalline and contains the anatase phase in the as-coated case. The top-view SEM image of the as-coated layer displays densely packed fine columnar morphology of the layer (Figure 2, left). Further heat-treatment increases the anatase crystallinity. At around 800 °C, the first indication of anatase-rutile transformation can be seen (Figure 3). After 3 h of heat-treatment at 1000 °C, full conversion to rutile takes place. The Al-doped TiO₂ layers which were used for sensor testing were calcined at 800 °C and, thus, contained mainly anatase phase and some minor amounts of rutile. The SEM top-view micrograph of the 800 °C heat-treated Al-doped layer indicates the crystallization development yielding some porosity at the grain and column boundaries (Figure 2, right). The sensor tests of Al-doped TiO₂ layers towards NO₂ were published in details elsewhere [10]. The most striking observation with this high-temperature sensor material was the alteration of the sensor signal direction at 800 °C yielding a resistance decrease under NO₂ exposure being opposite to the resistance increase observed at 600 °C (see Figure 4). No significant effect of humidity on the sensor response was observed at these temperatures.

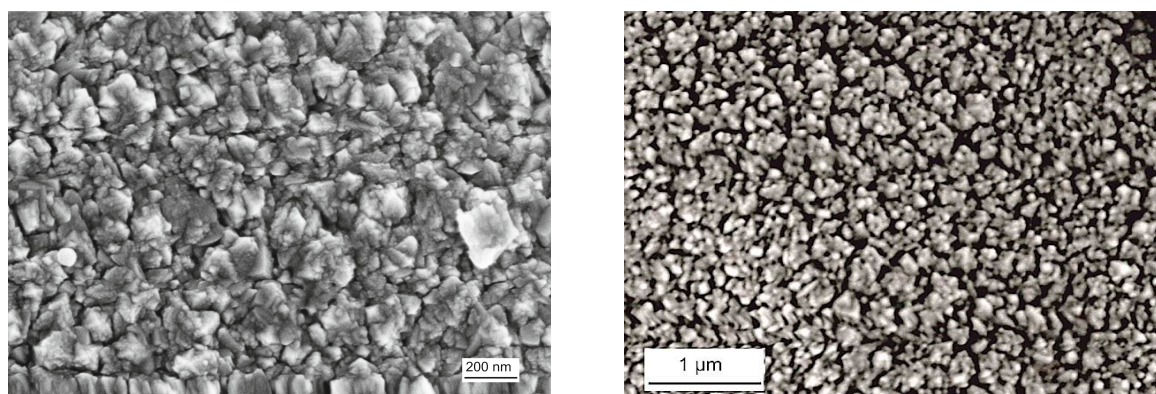


Figure 2. Top-view SEM micrographs of the sputter-coated Al-doped TiO₂ layer in the as-coated case (left), and after heat-treatment at 800 °C for 3 h in air (right).

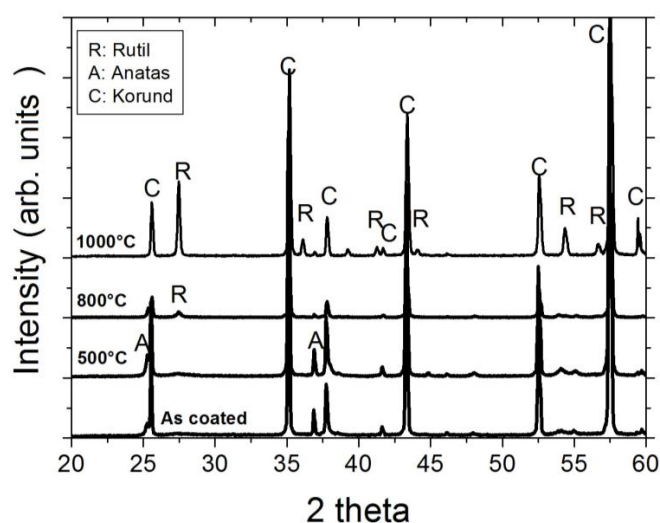


Figure 3. XRD diffractograms of the Al-doped TiO₂ layers deposited by a sputtering process in the as-coated state and *ex situ*, heat-treated at 500 °C, 800 °C, and 1000 °C.

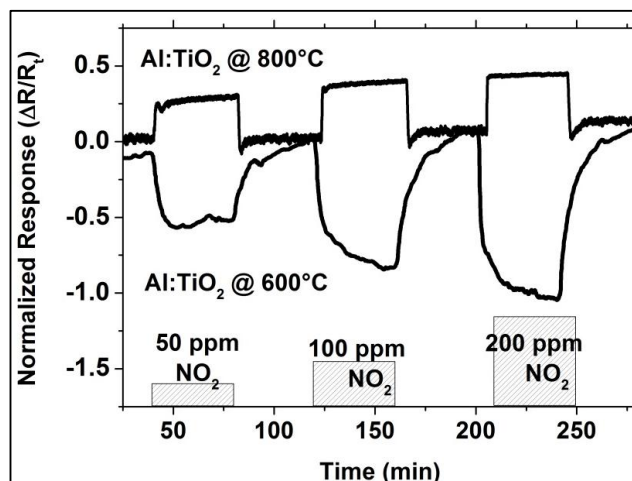


Figure 4. NO₂ response of Al-doped TiO₂ in dry argon environment at 600 °C and 800 °C.

This behavior can be assumed to be due to the conversion of NO₂ to NO because of the above-mentioned and the Figure 5 illustrated thermodynamic equilibrium conditions which may result in the formation of ionized oxygen species (e.g., O²⁻-ion) taking over the control of sensing mechanism through surface adsorption (see Equation (2) and [10]):

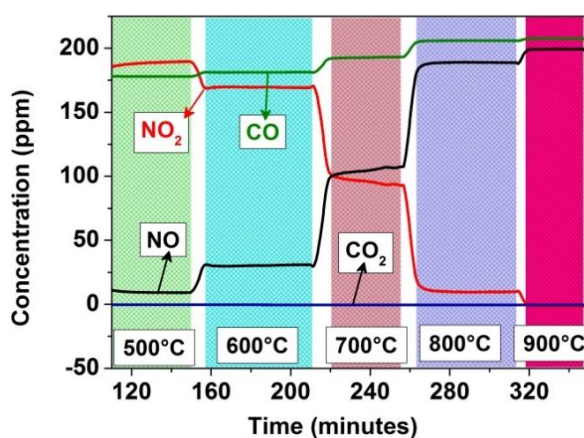
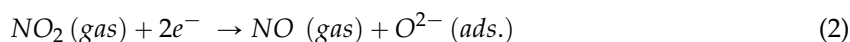


Figure 5. Temperature-dependent conversion of NO₂ to NO in the empty sensor test chamber, with no visible conversion of CO to CO₂.

This behavior of the Al-doped TiO₂ layer indicates poor NO₂-sensing capability at temperatures above 600 °C. On the other hand, Al-doped TiO₂ shows negligible sensitivity towards CO concentrations varying from 50 to 200 ppm in the given temperature range. Moreover, these layers are more sensitive to NO₂ when NO₂ and CO are simultaneously present in the test environment, indicating a minimized cross-sensitivity towards CO [9].

In order to overcome the NO₂ sensing deficit of the Al-doped TiO₂ layer, a perovskite layer as a catalytic filter is employed. This Rh-incorporating perovskite has a self-regenerative property which results in the segregation of Rh nanoparticles on the reduction and re-incorporation into the lattice upon oxidation [25]. Relying on the NO oxidizing capability of Rh, the effects caused on a sensor due to the high-temperature deviations in NO₂ containing gas environments can be eliminated.

3.2. Catalytic $\text{BaTi}_{0.95}\text{Rh}_{0.05}\text{O}_3$ Powder

The SEM observations of the $\text{BaTi}_{0.95}\text{Rh}_{0.05}\text{O}_3$ catalytic material exhibited that under oxidized conditions (e.g., after calcining at $1000\text{ }^\circ\text{C}$ in air), large prismatic grains of perovskite were formed. In turn, on heat-treatment of the oxidized powder, this time under reduced conditions (e.g., $900\text{ }^\circ\text{C}$ in 2.5 vol.% H_2), Rh metallic particles segregates at the grain boundaries of the perovskite (Figure 6, left and right, respectively).

In situ high-temperature XRD analysis of pre-calcined powder in the range of RT- $1000\text{ }^\circ\text{C}$ -RT showed that the increase of temperature results in shifting of all X-ray diffraction peak positions of $\text{BaTi}_{0.95}\text{Rh}_{0.05}\text{O}_3$ to lower Bragg angles (2θ) due to expansion of the lattice (see Figure 7). After heating to $700\text{ }^\circ\text{C}$ in air, the $\text{BaTi}_{0.95}\text{Rh}_{0.05}\text{O}_3$ powder yields the BaTiO_3 perovskite, BaTi_2O_5 , and BaCO_3 phases.

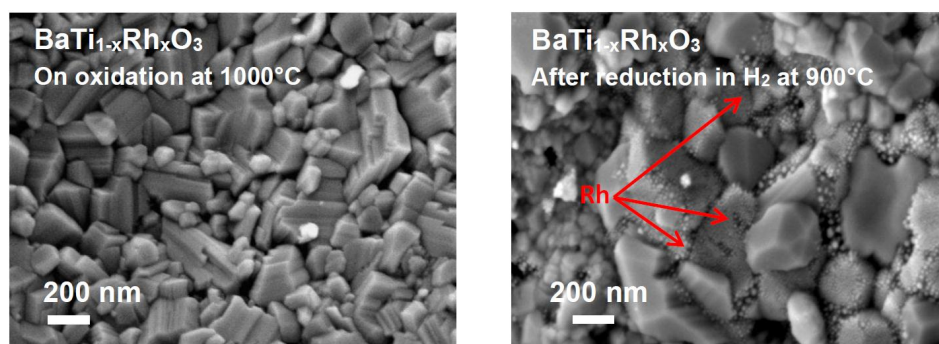


Figure 6. (Left) SE micrograph of the $\text{BaTi}_{0.95}\text{Rh}_{0.05}\text{O}_3$ catalytic filter after calcining at $1000\text{ }^\circ\text{C}$ in air and (Right) after reducing treatment at $900\text{ }^\circ\text{C}$ under 2.5 vol.% H_2 in argon, displaying the segregation of Rh nanoparticles.

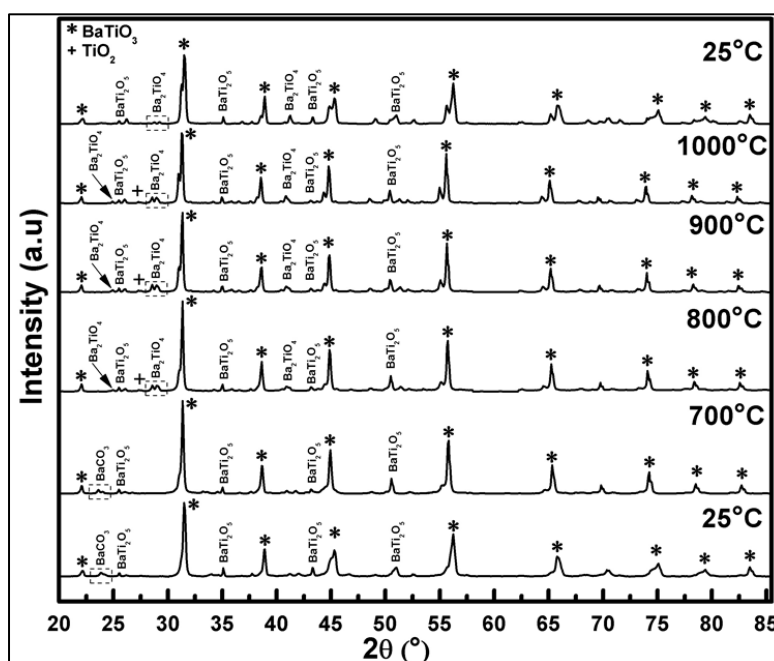


Figure 7. *In-situ* HT-XRD diffractograms of $\text{BaTi}_{0.95}\text{Rh}_{0.05}\text{O}_3$ powder collected over a temperature range varying from $25\text{ }^\circ\text{C}$ to $1000\text{ }^\circ\text{C}$ and cooling back to $25\text{ }^\circ\text{C}$.

BaCO_3 disappears at around $800\text{ }^\circ\text{C}$, probably due to the low melting point of the compound. In turn, at this temperature, Ba_2TiO_4 phase appears to form. On heating to $1000\text{ }^\circ\text{C}$, next to the

well-crystallized BaTiO_3 , the BaTi_2O_5 , and Ba_2TiO_4 phases at lower intensity, and a trace TiO_2 phase are detected. At this stage, the presence of some trace amounts of RhO_2 cannot be ruled out even though the matching peak positions were not identified due to the overlapping. After cooling down to RT, the *in situ* to 1000 °C heated powder contains BaTiO_3 , BaTi_2O_5 , and the (111) plane of Ba_2TiO_4 phases.

In summary, it can be concluded that heating to 1000 °C and cooling down to RT in air of the $\text{BaTi}_{0.95}\text{Rh}_{0.05}\text{O}_3$ catalytic powder results in full decomposition of BaCO_3 and the formation of BaTi_2O_5 and Ba_2TiO_4 through the irreversible phase conversion. These phases may contain partially-incorporated Rh. No clear identification of the presence of metallic Rh or RhO_2 was possible during *in situ* X-ray of this in air heat-treated powder.

After reduction treatment in H_2 , $\text{BaTi}_{0.95}\text{Rh}_{0.05}\text{O}_3$ perovskite powder displays fine agglomerates which are associated with the presence of metallic Rh (Figure 6, right). The presence of cubic Rh with the 2θ position of 47.8° in the X-ray diffraction pattern of the reduced perovskite powder indicates that the hexagonal perovskite decreased upon reduction in H_2 . The sensor tests were carried out with a $\text{BaTi}_{0.95}\text{Rh}_{0.05}\text{O}_3$ powder which was calcined in air at 1000 °C.

In order to understand the contribution of $\text{BaTi}_{0.95}\text{Rh}_{0.05}\text{O}_3$ perovskite to the sensor response, initially the sensor response of this perovskite has been recorded. For that, some interdigital sensor platforms were coated by screen-printing with a thick $\text{BaTi}_{0.95}\text{Rh}_{0.05}\text{O}_3$ perovskite powder. These sensors were tested towards NO_2 and CO in the form of single gas exposures having different concentrations at 600 °C to 900 °C in a dry argon environment (see Figure 8).

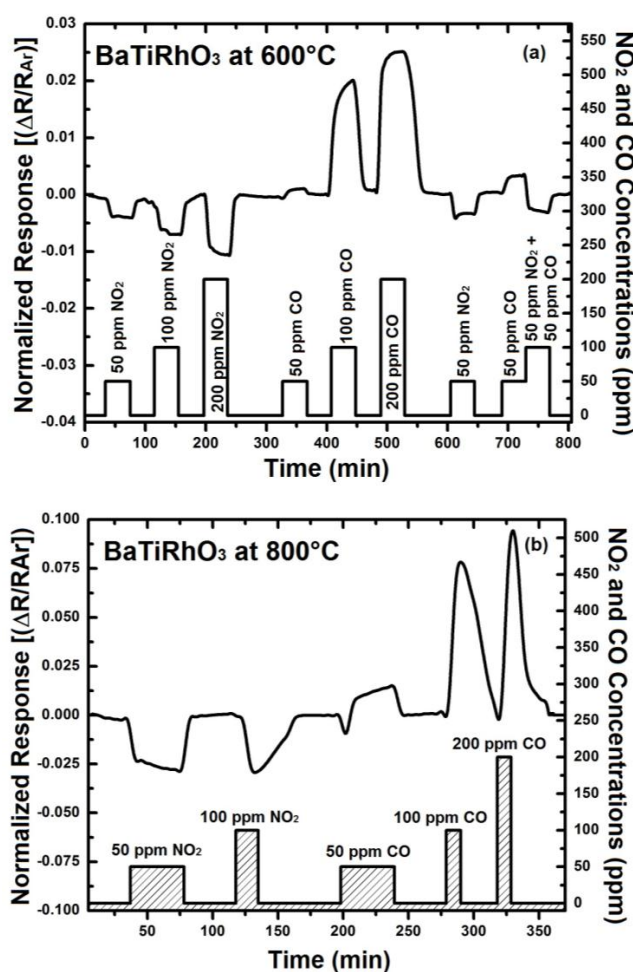


Figure 8. Cont.

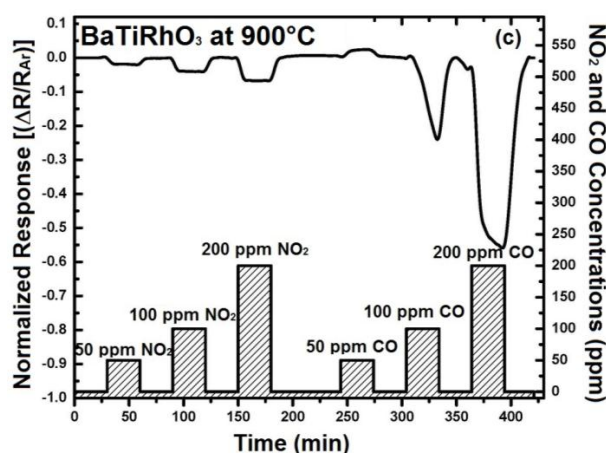


Figure 8. Sensor response of the $\text{BaTi}_{0.95}\text{Rh}_{0.05}\text{O}_3$ catalyst layer towards NO_2 and CO at 600 °C (a) 800 °C (b), and at 900 °C (c) in dry argon.

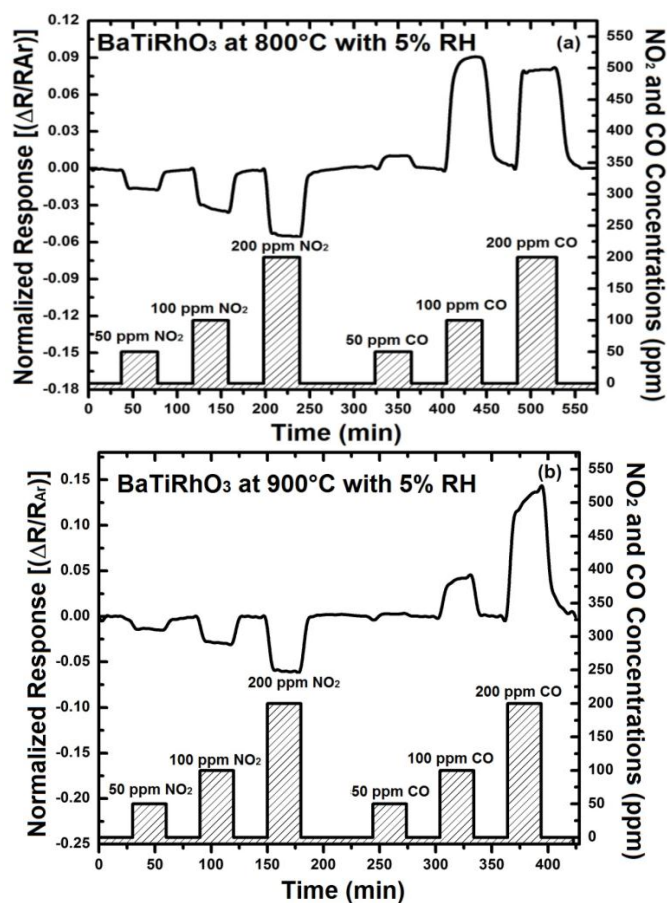


Figure 9. (a) Sensor response of only $\text{BaTi}_{0.95}\text{Rh}_{0.05}\text{O}_3$ thick catalytic layer towards NO_2 at 800 °C, and (b) at 900 °C in the presence of 5% humidity.

Thick layers of $\text{BaTi}_{0.95}\text{Rh}_{0.05}\text{O}_3$ perovskite catalyst yield remarkable response towards NO_2 at the temperatures of 600 °C to 900 °C and in dry argon, but also a high sensor response towards CO (50 to 200 ppm). As the sensor response towards NO_2 and CO improves with the temperature, the CO response alters to the opposite direction at 900 °C (see Figure 8). This behavior of the catalytic

layer may be due to the CO-oxidation capability. Our previous unpublished tests carried out with this catalytic perovskite by using 1% CO, 5000 ppm O₂ diluted in He indicated a very low light-off temperature for CO oxidation (below 210 °C). While under less oxygen-containing conditions, *i.e.*, by exposing the perovskite to 1000 ppm CO and 1000 ppm NO in He, it was observed that CO conversion occurs at significantly higher temperatures.

The addition of 5% humidity to the argon environment results in an improvement of the NO₂ response of BaTi_{0.95}Rh_{0.05}O₃ perovskite by a factor of two at 800 °C (e.g., 0.02 *vs.* 0.04 for 100 ppm at 800 °C) and somewhat less at 900 °C (see Figure 9). Similarly, CO response in the presence of humidity yields resistance increase at 900 °C, as observed under dry conditions, indicating an adsorption promotion effect of OH^{-δ} ions (see [14]). The discrepancy, concerning CO response at 900 °C under dry conditions, can be explained with the facts that water vapor or OH⁻ ions at this temperature may either react with CO during adsorption on the catalyst surfaces or the BaTi_{0.95}Rh_{0.05}O₃ influences catalytically the adsorption mechanism of CO under oxidizing conditions. All sensor responses with BaTi_{0.95}Rh_{0.05}O₃ were p-type at all test temperatures with the exception of CO exposure at 900 °C. Nevertheless, the sensor response towards CO is significant. Thus, considering this fact, it is expected that the BaTi_{0.95}Rh_{0.05}O₃ layers as a gas sensing material may display a high CO cross-interference under exposure to CO concentrations higher than 50 ppm at high temperatures.

3.3. NO₂ Response of BaTi_{0.9}Rh_{0.1}O₃ Catalyst + Al-Doped TiO₂ Duplex Layers

According to the concept presented above in Section 2.1, duplex sensor layers having catalytic BaTi_{0.95}Rh_{0.05}O₃ perovskite and Al-doped TiO₂ are tested for their NO₂-response in the temperature range of 600 °C to 900 °C.

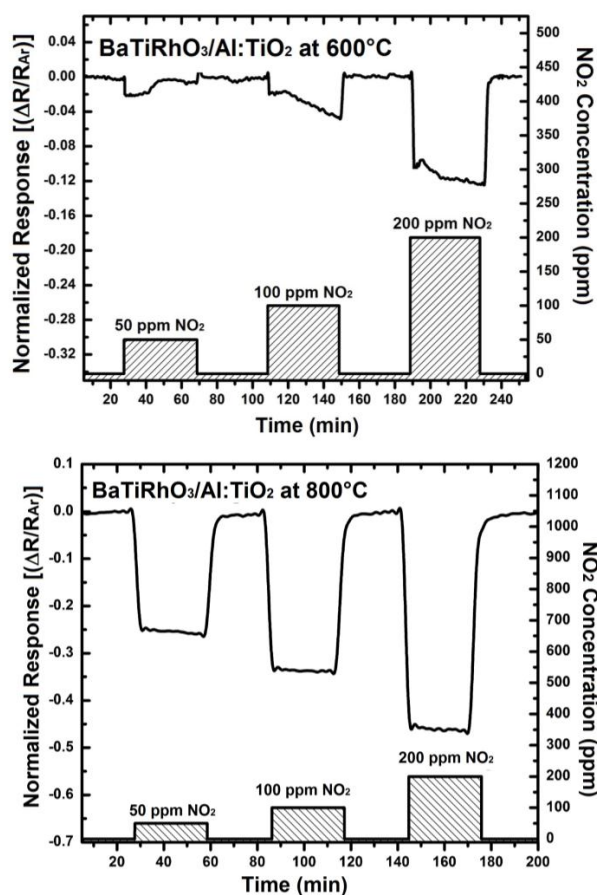


Figure 10. *Cont.*

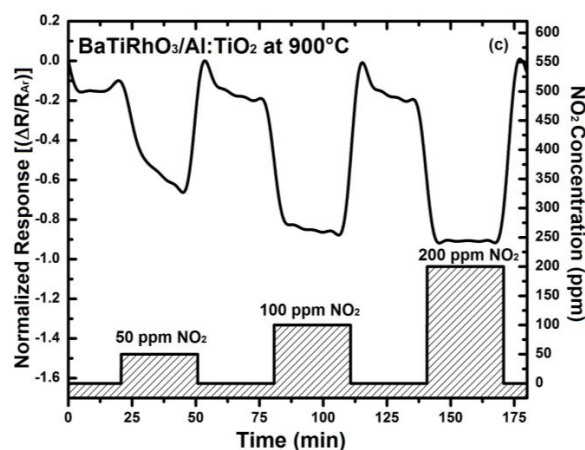


Figure 10. Sensor response of $\text{BaTi}_{0.95}\text{Rh}_{0.05}\text{O}_3$ catalyst + Al-doped TiO_2 sensor duplex layers towards NO_2 in a dry argon environment at $600\text{ }^\circ\text{C}$ (a), at $800\text{ }^\circ\text{C}$ (b), and at $900\text{ }^\circ\text{C}$ (c).

The NO_2 sensor response obtained with these duplex layers display remarkable sensitivity values at $600\text{ }^\circ\text{C}$, $800\text{ }^\circ\text{C}$, and $900\text{ }^\circ\text{C}$ despite high gas temperatures (e.g., 0.12 at $600\text{ }^\circ\text{C}$, 0.46 at $800\text{ }^\circ\text{C}$, and 0.92 at $900\text{ }^\circ\text{C}$, upon exposure to 200 ppm), (see Figure 10). Moreover, the change in signal direction which was observed with the Al-doped TiO_2 layer as indicated with the sensor responses given in Figure 4 does not occur when duplex sensing layers are employed.

In order to clarify whether this response at such elevated temperatures is from NO_2 or from NO , the sensor response of this duplex layer towards NO was recorded in dry synthetic air (see Figure 11). Normally as shown with Figure 5, above $600\text{ }^\circ\text{C}$ under dry conditions, a temperature-dependent conversion of NO_2 to NO occurs.

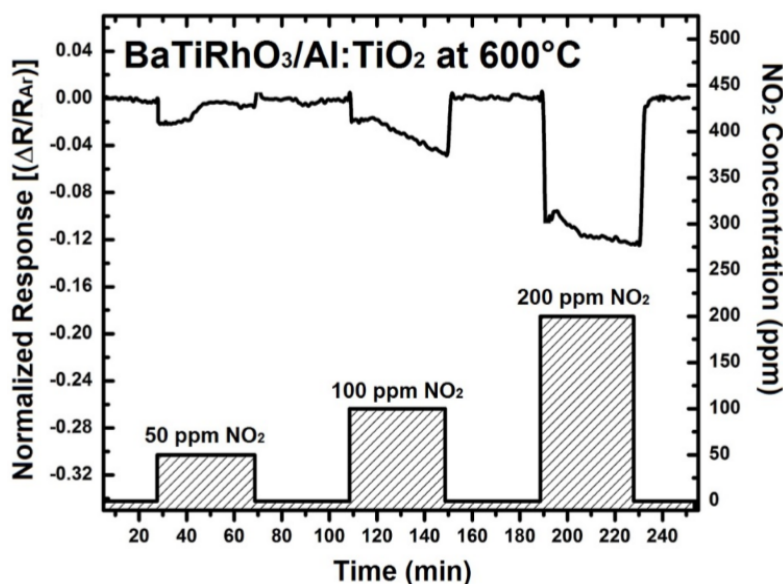


Figure 11. Sensor response of $\text{BaTi}_{0.95}\text{Rh}_{0.05}\text{O}_3$ catalytic + Al-doped TiO_2 sensor duplex layers at $600\text{ }^\circ\text{C}$ toward NO in a dry synthetic air environment.

The sensor tests of the $\text{BaTi}_{0.95}\text{Rh}_{0.05}\text{O}_3$ perovskite and Al-doped TiO_2 duplex layer carried out toward NO in a dry synthetic air environment at $600\text{ }^\circ\text{C}$ exhibited significantly lower sensitivity values (e.g., 0.018 and 0.023 under exposure to 50 ppm and 200 ppm, respectively). Further analyses, which were carried out to observe the effect of catalytic perovskite powder on NO_2/NO conversion at high

temperatures, indicated that full NO_2 to NO conversion already occurs at $300\text{ }^\circ\text{C}$ if $\text{BaTi}_{0.95}\text{Rh}_{0.05}\text{O}_3$ catalytic powder was exposed to 200 ppm NO_2 in the sensor chamber (see Figure 12). In turn, when the chamber is empty, *i.e.*, without the perovskite catalyst, the NO_2 -to- NO conversion develops gradually, starting from $500\text{ }^\circ\text{C}$, and is completed above $800\text{ }^\circ\text{C}$ as, at that temperature, no more NO_2 can be measured in the system's output (see Figure 5). Thus, it is reasonable to assume that the $\text{BaTi}_{0.95}\text{Rh}_{0.05}\text{O}_3$ catalytic top layer conditions the test environment to have $\text{NO}+\text{O}^{2-}$ at all test temperatures and catalytically oxidizes NO to NO_2 at the interface of the perovskite and the Al-doped TiO_2 layer [10]. Thus it can be concluded that exposure of the sensor to NO_2 at higher temperatures yields a sensor signal which cannot be correlated to NO and to molecular oxygen from the synthetic air, but to NO_2 .

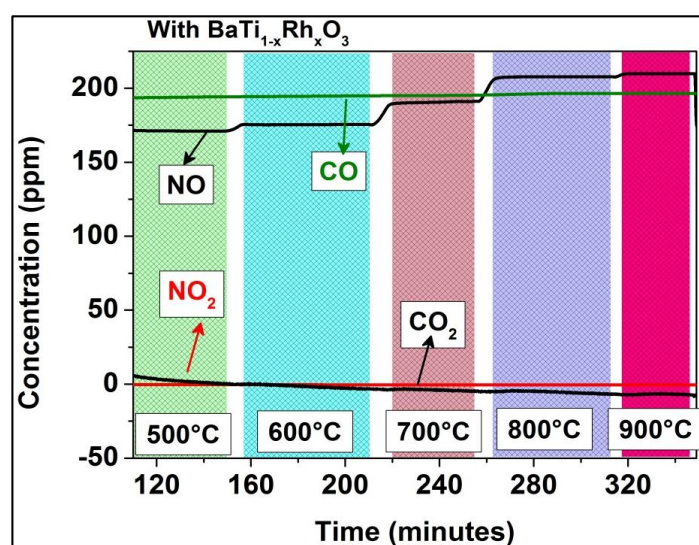


Figure 12. Temperature-dependent conversion of NO_2 and CO with $\text{BaTi}_{0.95}\text{Rh}_{0.05}\text{O}_3$ catalytic powder present in the test chamber.

Table 1 summarizes a selection of sensor properties of single and duplex sensor layers investigated in this study. For comparison purposes, only the responses toward 200 ppm NO_2 are considered. Sensitivities of $\text{Al}:\text{TiO}_2$ single layer and $\text{BaTiRhO}_3/\text{Al}:\text{TiO}_2$ duplex layer are relatively high at $600\text{ }^\circ\text{C}$ (0.70 and 0.92, respectively), but the recovery of sensor response with the single $\text{Al}:\text{TiO}_2$ layer requires extremely longer times. At higher temperatures, and in a humid environment, this appears to be shortened. The sensor with the single BaTiRhO_3 layer exhibits, in turn, the lowest sensitivities (0.11 and 0.05) at all test temperatures ($600\text{--}900\text{ }^\circ\text{C}$). No further NO_2 -sensing measurement is carried out at $900\text{ }^\circ\text{C}$ with the single $\text{Al}:\text{TiO}_2$ layer because of the lack of reliability of its sensor signal.

Table 1. Sensor properties of various sensor layers in the temperature range of $600\text{--}900\text{ }^\circ\text{C}$ in dry or in 5% humid argon environment.

Sensing Layer vs. 200 ppm NO_2	Gas Temperature ($^\circ\text{C}$)	Carrier Gas (Argon) Environment	Sensitivity	Reaction Time (min)	Recovery Time (min)
$\text{Al}:\text{TiO}_2$	600	dry	0.76	3.0	13.0
$\text{Al}:\text{TiO}_2$	600	5% humidity	0.69	2.5	17.0
$\text{BaTiRhO}_3/\text{Al}:\text{TiO}_2$	600	5% humidity	0.92	2.0	4.3
BaTiRhO_3	600	dry	0.11	2.2	3.4
$\text{Al}:\text{TiO}_2$	800	dry	0.50	3.7	22.0
$\text{Al}:\text{TiO}_2$	800	5% humidity	0.46	3.8	4.2
$\text{BaTiRhO}_3/\text{Al}:\text{TiO}_2$	800	5% humidity	0.16	1.6	2.5
BaTiRhO_3	800	5% humidity	0.050	3.7	8.3
BaTiRhO_3	800	dry	0.052	7.3	7.6
BaTiRhO_3	900	5% humidity	0.053	3.4	4.5
$\text{BaTiRhO}_3/\text{Al}:\text{TiO}_2$	900	5% humidity	0.061	3.2	4.3

The sensitivity of the sensor with the duplex layer reduces down to 0.16 at 800 °C, and further to 0.06 at 900 °C. Although the sensitivity of the duplex layer sensor (*i.e.*, BaTiRhO₃/Al:TiO₂) is lower than that of the Al:TiO₂ single layer, the reaction and recovery times of the sensor with the duplex layer is partly to half as short than those of the Al:TiO₂ single layer sensor (reaction times = 2.0 min *vs.* 2.5 min at 600 °C and 1.6 min *vs.* 3.8 min at 800 °C, recovery times = 4.3 min *vs.* 17 min at 600 °C and 2.5 min *vs.* 4.2 min at 800 °C, respectively). The sensitivities and the reaction and recovery times of the BaTiRhO₃/Al:TiO₂ duplex layer sensor remain in the same range at all test temperatures, indicating a maintained reliability with this sensor.

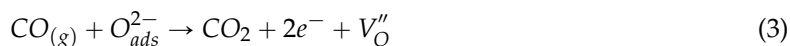
Humidity shows no significant effect on sensitivity, although some influence on reaction and recovery times are observed favoring humidity at 800 °C, and oppositely at 600 °C. Therefore, it is not possible to identify any specific trend regarding the humidity influence. Although it is obvious that the BaTiRhO₃ catalytic layer intervenes in the thermodynamic equilibrium condition of NO₂/NO environment by lowering the conversion temperature significantly, as a single sensor layer, the sensor with the BaTiRhO₃ single layer does not yield good performance for NO₂-sensing.

The literature indicates that perovskites with different formulations give great opportunity to detect gas mixtures by means of sensor arrays. Doping elements either in the lattice of perovskite or on the surface of perovskite could help to improve sensing performance of perovskite oxide and to decrease the sensing temperature [27,28]. La-based, Ce and Pd-doped perovskites are proven to yield good sensing behavior toward CO and CH₄, respectively. No other sensor study is known to date with the BaTiRhO₃ catalytic layer to confirm its behavior. However, Figure 9 displays that the sensor with a single BaTiRhO₃ layer yields greater signals toward CO than NO₂.

The sensors with the BaTiRhO₃/Al:TiO₂ duplex layers, in turn, exhibit a NO₂-selective sensing as exposed to CO + NO₂ mixed gas environments in the temperature range of 600 °C and 900 °C. Although stronger signals are observed by exposure only to CO, it appears that these signals are in the same direction as those toward NO₂ (Figure 13). Usually, the semiconducting sensors yield signals in opposite directions when exposed to oxidizing (e.g., NO₂, O₂) and reducing gases (e.g., CO, CH₄).

Previous studies which used XPS to determine the nature of CO adsorption on the surface of doped LaCoO₃ perovskite formulations as the sensor material have revealed that CO preferentially adsorbs on the lattice oxygen in the form of mono-dentate carbonate on the surface of perovskite-type oxide. Ce (e.g., La_{0.9}Ce_{0.1}CoO₃) doping changed not only the total amount of adsorbed CO but also the nature of adsorption phenomena. By adding Ce, in addition to the mono-dentate form, the bi-dentate carbonate form was also appeared on the surface resulting in an increase of the total adsorbed CO [27]. In the case of Pd-doped LaFeO₃, the noble metal gives an active site on the metal oxide to adsorb methane species. Pd is well known for its H dissolving capacity, which could help to create PdH pair in methane adsorption phenomena [28].

In our case, it is likely that under single CO gas exposure in dry argon, CO adsorption rapidly consumes the surface-adsorbed oxygen of the sensing layer forming CO₂ and excess electrons according to Equation (3):



Hence, it is probable that the sensors with the duplex layer exhibit CO cross-interference. In order to test this, the sensor response of the BaTi_{0.95}Rh_{0.05}O₃ catalyst + Al-doped TiO₂ duplex layers was recorded under NO₂ and CO single-gas exposure, followed by NO₂ and CO mixed gas exposure at 800 °C and 900 °C (Figure 13 left and right). These tests displayed that the duplex layer is more sensitive to NO₂ in the presence of CO, while under CO single-gas exposure, relatively high sensor sensitivity is recorded. The resistance decrease obtained on exposure to gas mixtures of 50 ppm NO₂ + 50 ppm CO, 100 ppm NO₂ + 100 ppm CO, and 200 ppm NO₂ + 200 ppm CO equals to that obtained by exposure only to NO₂ at concentrations of 50, 100, and 200 ppm, respectively. In turn, under NO₂ + CO gas mixture exposure, NO₂ is converted to NO + O²⁻ at temperatures above 300 °C through the BaTi_{0.95}Rh_{0.05}O₃ catalytic layer and this ionized oxygen may readily react with CO without being in interaction with the sensor surface and is removed as CO₂, while the converted NO reacts

with the oxygen adsorbed on the surface of Al-doped TiO₂ sensing layer. Thus, at temperatures as high as 800 °C and 900 °C, the sensor with the BaTiRhO₃/Al:TiO₂-duplex layer gives signals preferentially corresponding to NO₂, despite being exposed to CO + NO₂ gas mixtures at relatively higher concentrations (Figure 13, left and right).

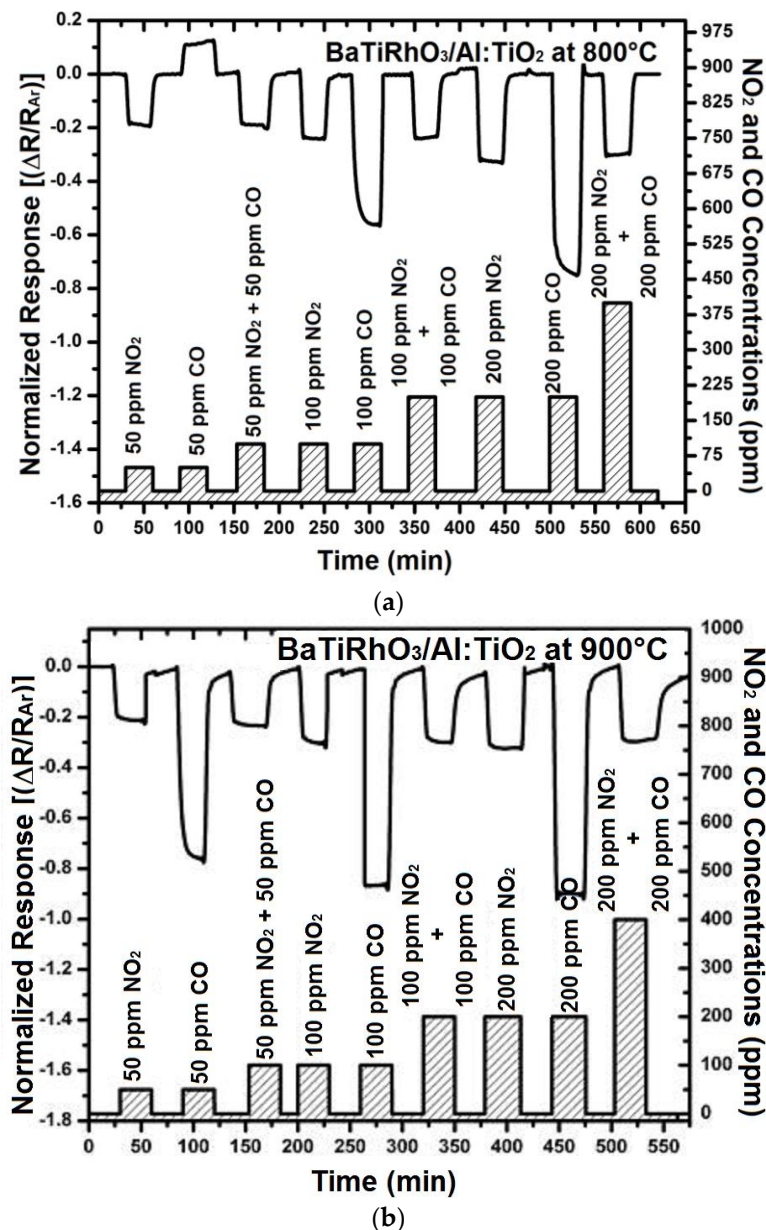


Figure 13. Sensor response of BaTi_{0.95}Rh_{0.05}O₃ catalyst + Al-doped TiO₂ duplex layers at 800 °C (a) and 900 °C (b) in dry argon environment on exposure to NO₂ and CO single and/or NO₂ + CO gas mixtures.

4. Conclusions

Trivalent doping of TiO₂ enables sensor response towards NO₂ at temperatures up to 800 °C. However, above 600 °C, a change in the direction of the sensor signal is observed. This behavior of TiO₂ sensors can be eliminated by coating the sensor layers with a BaTi_{0.95}Rh_{0.05}O₃ catalytic filter layer to obtain a reliable sensor response at temperatures as high as 900 °C. The BaTi_{0.95}Rh_{0.05}O₃ layer catalytically converts NO₂ to NO already above 300 °C and, thus, conditions the sensor

environment by formation of ionized oxygen allowing a sensor response with descent sensitivity. Moreover, CO interference is eliminated by using $\text{BaTi}_{0.95}\text{Rh}_{0.05}\text{O}_3$ as a catalytic filter for sensing NO_2 in the CO + NO_2 -mixed gas environments. However, it is not clear if solely the precious metal, Rh, which is present in the $\text{BaTi}_{0.95}\text{Rh}_{0.05}\text{O}_3$ perovskite is responsible for this conditioning or an interaction with the perovskite lattice occurs. In order to clarify this, the tests must be carried out using a catalytic filter made of pure BaTiO_3 perovskite on the Al-doped TiO_2 layer. Conventional TWC catalyst cannot be used for this purpose (*i.e.*, as a catalytic filter) due to the lack of necessary electrical conductivity.

Acknowledgments: The authors acknowledge the financial support of DFG under the contract number SA 1343/5. The valuable scientific comments of W. Grünert of the Ruhr-University-Bochum are gratefully acknowledged.

Author Contributions: B.S., A.Y. and G.C.M.R. conceived and designed the experiments; A.Y., G.C.M.R and A.A.H. performed the experiments; B.S., A.A.H and E.C. analyzed the data; E.C. contributed XRD analysis; B.S. wrote the paper.

Conflicts of Interest: The authors declare no conflict of interest.

References

1. Baukal, C. Everything you need to know about NOx: Controlling and minimizing pollutant emissions is critical for meeting air quality regulations. *Metal. Finish.* **2005**, *103*, 18–24. [[CrossRef](#)]
2. Glassman, I.; Yetter, R.A. *Combustion*, 4th ed.; Academic Press: Burlington, MA, USA, 2007.
3. Global Digital Central, Thermal Fluidspedia. Available online: <https://www.thermalfluidscentral.org/encyclopedia/index.php/Basics> (Combustion) (accessed on 31 March 2016).
4. DieselNet Technology Guide, Gasous Emissions. Available online: https://www.dieselnets.com/tech/emi_gas.php (accessed on 31 March 2016).
5. European Commission, Environment. Available online: <http://ec.europa.eu/environment/air/quality/standards.htm> (accessed on 31 March 2016).
6. United States Department of Labor. Available online: https://www.osha.gov/dts/chemicalsampling/data/CH_257400.html (accessed on 31 March 2016).
7. The State of Nevada, Department of Motor Vehicles. Available online: http://dmv.nv.com/emission_obd.htm (accessed on 31 March 2016).
8. Yamazoe, N.; Shimano, K. Theory of power laws for semiconductor gas sensors. *Sens. Actuators B: Chem.* **2008**, *128*, 566–573. [[CrossRef](#)]
9. Gardon, M.; Guilemany, J.M. A review on fabrication, sensing mechanisms and performance of metal oxide gas sensors. *J. Mater. Sci.: Mater. Electron.* **2013**, *24*, 1410–1421. [[CrossRef](#)]
10. Saruhan, B.; Yüce, A.; Gönüllü, Y.; Kelm, K. Effect of Al doping on NO_2 gas sensing of TiO_2 at elevated temperatures. *Sens. Actuators B: Chem.* **2013**, *187*, 586–597. [[CrossRef](#)]
11. Barsan, N.; Koziej, D.; Weimer, U. Metal oxide-based gas sensor research: How to? *Sens. Actuators B: Chem.* **2007**, *121*, 18–35. [[CrossRef](#)]
12. Savage, N.O.; Akbar, S.A.; Dutta, P.K. Titanium dioxide based high temperature carbon monoxide selective sensor. *Sens. Actuators B: Chem.* **2001**, *72*, 239–248. [[CrossRef](#)]
13. Kim, B.; Lu, Y.; Hannon, A.; Meyyappan, M.; Li, J. Low temperature Pd/ SnO_2 sensors for CO detection. *Sens. Actuators B: Chem.* **2013**, *177*, 770–775. [[CrossRef](#)]
14. Haidry, A.A.; Kind, N.; Saruhan, B. Investigating the influence of Al-doping and background humidity on NO_2 sensing characteristics of magnetron sputtered SnO_2 sensors. *J. Sens. Syst.* **2015**, *4*, 271–280. [[CrossRef](#)]
15. Gönüllü, Y.; Haidry, A.A.; Saruhan, B. Nanotubular Cr-doped TiO_2 for use as high-temperature NO_2 -selective gas sensor. *Sens. Actuators B: Chem.* **2015**, *217*, 78–87. [[CrossRef](#)]
16. Gönüllü, Y.; Kelm, K.; Mathur, S.; Saruhan, B. Equivalent Circuit Analysis of Impedance Response for Cr-doped TiO_2 -NTs towards NO_2 Gas. *Chemosensors* **2014**, *2*, 69–84. [[CrossRef](#)]
17. Gönüllü, Y.; Mondragón Rodríguez, C.G.; Saruhan, B.; Ürgen, M. Improvement of gas sensing performance of TiO_2 towards NO_2 by nano-tubular structuring. *Sens. Actuators B: Chem.* **2012**, *169*, 151–160. [[CrossRef](#)]
18. Galstyan, V.; Comini, E.; Faglia, G.; Sberveglieri, G. TiO_2 Nanotubes: Recent Advances in Synthesis and Gas Sensing Properties. *Sensors* **2013**, *13*, 14813–14838. [[CrossRef](#)] [[PubMed](#)]

19. Spencer, M.J.S. Gas sensing applications of 1D-nanostructured zinc oxide: Insights from density functional theory calculations. *Prog. Mater. Sci.* **2012**, *57*, 437–486. [[CrossRef](#)]
20. Park, S.; Kim, S.; Park, S.; Lee, W.; Lee, C. Effects of functionalization of TiO₂ nanotube array sensors with Pd nanoparticles on their selectivity. *Sensors* **2014**, *14*, 15849–15860. [[CrossRef](#)] [[PubMed](#)]
21. Rzyhikov, A.; Latheau, M.; Gaskov, A. Al₂O₃ (M=Pt, Ru) catalytic membranes for selective semiconductor gas sensors. *Sens. Actuators B: Chem.* **2005**, *109*, 91–96. [[CrossRef](#)]
22. Cabot, A.; Arbiol, J.; Cornet, A.; Morante, J.R.; Chen, F.; Liu, M. Mesoporous catalytic filters for semiconductor gas sensors. *Thin Solid Films* **2003**, *436*, 64–69. [[CrossRef](#)]
23. Khodadadi, A.; Mohajezadeh, S.S.; Mortazavi, Y.; Miri, A.M. Cerium oxide/SnO₂-based semiconductor gas sensors with improved sensitivity to CO. *Sens. Actuators B: Chem.* **2001**, *80*, 267–271. [[CrossRef](#)]
24. Hübner, M.; Yüce, A.; Mondragón-Rodríguez, C.G.; Saruhan, B.; Barsan, N.; Weimar, U. BaTi_{0.95}Rh_{0.05}O₃ catalytic filter layer—A promising candidate for the selective detection of CO in the presence of H₂. *Procedia Eng.* **2010**, *5*, 107–110. [[CrossRef](#)]
25. Saruhan, B.; Mondragón Rodríguez, C.G.; Yüce, A.; Haidry, A.A.; Heikens, S.; Grünert, W. Integrated performance monitoring of three-way catalytic converters by self-regenerative and adaptive high temperature catalyst and sensors. *Adv. Eng. Mater.* **2015**. [[CrossRef](#)]
26. Mondragón Rodríguez, G.C.; Gönüllü, Y.; Ferri, D.; Eyssler, A.; Otal, E.; Saruhan, B. Phase transitions of BaTi_{0.9}Rh_{0.1}O₃ perovskite-type oxides under reducing environments. *Mater. Res. Bull.* **2014**, *61*, 130–135. [[CrossRef](#)]
27. Ghasdi, M.; Alamdari, H.; Royer, S.; Adnot, A. Electrical and CO gas sensing properties of nanostructured La_{1-x}Ce_xCoO₃ perovskite prepared by activated reactive synthesis. *Sens. Actuators B: Chem.* **2001**, *156*, 147–155. [[CrossRef](#)]
28. Ghasdi, M.; Alamdari, H. CO sensitive nanocrystalline LaCoO₃ perovskite sensor prepared by high energy ball milling. *Sens. Actuators B: Chem.* **2010**, *148*, 478–485. [[CrossRef](#)]



© 2016 by the authors; licensee MDPI, Basel, Switzerland. This article is an open access article distributed under the terms and conditions of the Creative Commons Attribution (CC-BY) license (<http://creativecommons.org/licenses/by/4.0/>).